International Journal of the Physical Sciences Vol. 6(6), pp. 1379-1387, 18 March, 2011
Available online at http://www.academicjournals.org/IJPS
DOI: 10.5897/IJPS11.078
ISSN 1992 - 1950 ©2011 Academic Journals

Full Length Research Paper

A depth-averaged two-dimensional model for flow around permeable pile groins

Jung-Tai Lee[1], H. C. Chan[2], Chin-Kun Huang[3], Yu-Min Wang[4] and Wei-Che Huang[4]

[1]Sinotech Engineering Consultants, LTD. Geotechnical Engineering Department, 12F, 171, Nanking E. Rd. Sec.5, Taipei 10570, Taiwan (Republic of China).
[2]Department of Soil and Water Conservation, National Chung Hsing University, 250 Kuo Kuang Rd., Taichung 402, Taiwan (Republic of China).
3Department of Hydraulic and Ocean Engineering, National Cheng Kung University, No. 1, University Rd., Tainan 70101, Taiwan (Republic of China).
[4]Department of Civil Engineering, National Pingtung University of Science and Technology, No. 1, Shuefu Road, Neipu, Pingtung 91201, Taiwan (Republic of China).

Accepted 25 February, 2011

Results of a comparison between *in-situ* experiment and numerical modelling for flow around permeable pile groins were presented. The groin sets consisted of porous-fence piles with a diameter of 1.0 m and were conducted in the Laonong River, Southern Taiwan. A numerical model that solved depth-averaged RANS (Reynolds-averaged Navier-Stokes equations) and the continuity equation was developed to simulate the flow around the permeable pile groins. The turbulent effects were determined by the standard $k-\varepsilon$ turbulence model. Drag forces exerted by the flow on the permeable pile groins were considered by adding source terms into momentum equations. The numerical predictions showed good agreement with the experimental results. The present model captured important flow features that were critical for characterizing the engineering design. Furthermore, the influence of different discharges on the hydrodynamic characteristics of permeable pile groins was investigated by using the present model. When the flow passed through the permeable pile groins, flow velocity reduced downstream of the groins and the water depth dropped significantly in the stream wise direction. It was observed that the levels of the flow velocity and water depth reduction decreased as the flow discharge increased. This was attributed to extra momentum transfer between the jet flows passing through the gaps between the permeable pile groins and the flow just behind the permeable pile groins.

Key words: Groins, shallow water, turbulent flow, numerical simulation.

INTRODUCTION

Groins are one of the oldest forms of hydraulic structures used in natural rivers or streams. Generally, traditional groins are solid structures, constructed using concrete, rocks, gravels or gabions, extending outward from a bank into a stream. These may be short or long, high or low, submerged or emergent groins, where the purpose is to deflect the current away from the bank to protect the banks from erosion or maintain navigation safety. It had been recognized that the flows around solid groins are very complex. Recirculation zones with strong shear layers are generated by the deflected flow passing the groins. A number of investigations have been conducted to study flow characteristics around solid-groin-like structures in laboratories or using numerical models (Rajaratnam and Nwachukwu, 1983; Jia and Wang, 1996; Ahmed and Rajaratnam, 2000; Barbhuiya and Dey, 2004; Yazdi et al., 2010). The diversified flows around groins are useful to preserve and maintain river ecosystems (Schwartz and Kozerski, 2003; Carling et al., 1996). The stagnant zone between the groins is a favorable location for fish with respect to reproduction and

*Corresponding author. E-mail: hcchan@nchu.edu.tw. Tel: 886-4-2284-0381 ext 118.

as a habitat, whereas the shallowness and low flow velocities give rise to sedimentation and the development of vegetation (Arlinghaus et al., 2002; Armstrong et al., 2003). In the cases of ecological richness, the complex flows around groins play an important role in the increase of the variety of habitats for aquatic biota (Shields et al., 1995; Bischoff and Wolter, 2001; Kruk, 2007). However, the local scour around the groin toes formed from the complex flows may also cause the failure of groins (Kwan and Melville, 1994). The excessive local scour is undesired with respect to the stability of the groin structure.

As an improvement to traditional solid groins, the depth of the local scour hole around the permeable groin is lower than the respective one of the solid groin (Teraguchi et al., 2008). The permeable pile groins, composed of rows of piles, are increasingly used for the advantages of easy construction and low maintenance cost. Despite the widespread use of permeable pile groins, many aspects of their design are based on prior experience and are only applicable to streams of a similar nature (Abam, 1993). Little information related to the hydrodynamic properties of the permeable pile groins is available in previous studies. Abam (1994) studied the factors affecting performance of permeable groins by combining the properties of soil and flow related to the failure of overturning as a factor of safety. The most critical factor that determines groin stability is depth of the groin, followed by flow velocity and discharge, unit weight of the water, unit weight of the soil, and cohesion. Xu et al. (2006) presented numerical solutions for the characteristics of the bore pressure on pile groin by using a two-dimensional vertical model. However, the most common flow properties considered in practical engineering situations are plane variations and combinations of flow patterns. Uijttewaal (2005) measured the velocity and turbulence intensity of wake flow around various groins using particle tracking velocimetry (PTV). It was found that the turbulence properties near and downstream of the groins could be manipulated by changing the permeability and slope of the groin-head. Huang (2009) found that permeable groins set up at an angle of 30° resulted in the best diversion effect for preventing bank erosion.

The aforementioned literature demonstrates the richness of the detailed investigation of flow structures around solid groins, and their improvements to the river ecosystems have been emphasized. However, limited data exist for the case where the permeable groins are arranged near the river bank. A numerical model to improve the understanding of the complicated flow in the vicinity of permeable pile groins is expected to aid in the suitable design of such structures. In the present study, the flow characteristics around the permeable pile groins are studied numerically and experimentally. For the experiment, permeable pile groins are arranged in a river and the flow data are collected. A numerical model based on the RANS equations with a resistance law representing the permeable pile groins is developed to simulate the flow around permeable pile groins. The predicted results are compared with the experimental results in order to validate the numerical model. Emphasis is given to the effects of the permeable pile groins on the velocities and turbulence quantities of the flow. Detailed processes, such as how the turbulent model is adapted and how the boundary conditions are imposed, as well as some computed findings are presented in this paper.

IN-SITU EXPERIMENT

The experiment was conducted at nearly straight reach in the Laonong River, Southern Taiwan. Picture 1 shows the groins after installation. The groins were laid out in a row of ten permeable piles. Each permeable pile consists of a pile, steel pipe, and porous fence. In order to overcome anticipated problems of stability, a pre-bored P.C. pile was selected and inserted into the riverbed to a depth of 10.0 m. On the top of the pile, the steel pipe was attached with the porous fence. Two sets of porous fence that measured 1.5 and 1.0 m in height, respectively, with the same diameter of 1.0 m, were used. Effective deflection of flow can be determined by the permeability of the porous fence. The 1.5-m-high piles were installed landward, while the 1.0-m- high piles were installed in the deeper sections. The pile groins were placed on the left side of the reach in the test reach at an angle of 30°. The crests of the groins were 1.0 to 1.5 m higher than the bed and were emergent at low flow and submerged at high flow. An electro-magnetic micro-velocimeter (Union Engineering, UECM-200A) was used to measure flow velocities during the experiment. Flow velocity and depth data were collected from the reach on July 7, 2009. Constant rate of discharge was observed and equal to 34.60 cm during the experiment. Flow velocities were measured at 2 cross sections (A1 and A2) on the x-y plane as shown in Figure 1. At each cross section, the measurements of surface velocity were made at 15 points in the transverse, with a distance of 2.0 m from the right side of the reach.

NUMERICAL MODEL

The numerical model used by the present study originally developed by Leu et al. (2008), was modified to include drag terms in the momentum equation. The numerical model used to simulate the flow field is based on fixed-bed conditions. The governing equations of the proposed numerical model are based on the depth-averaged RANS (Reynolds-averaged Navier-Stokes equations) and the continuity equation, which can be expressed as follows.

Continuity equation

$$\frac{\partial[(1-c)h]}{\partial t}+\frac{\partial[(1-c)uh]}{\partial x}+\frac{\partial[(1-c)vh]}{\partial y}=0 \quad (1)$$

Picture 1. Study reach, Laonong river, photo facing left bank. Black arrow denotes flow direction; red arrow indicates position for groin-head.

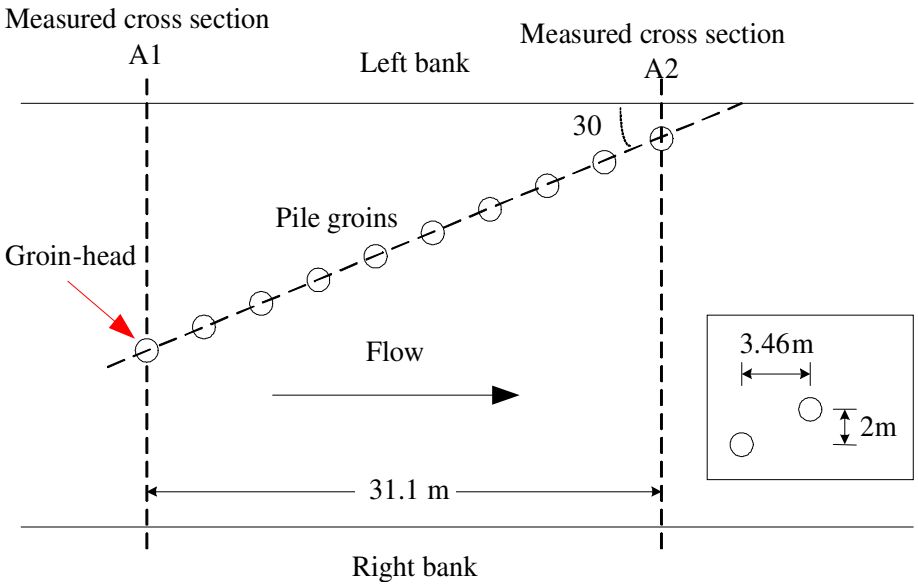

Figure 1. Details of permeable pile groins and measured cross sections of flow velocities.

Momentum equation

$$\frac{\partial[(1-c)uh]}{\partial t}+\frac{\partial[(1-c)uuh]}{\partial x}+\frac{\partial[(1-c)uvh]}{\partial y}$$
$$=-g(1-c)h\frac{\partial z_s}{\partial x}+\frac{1}{\rho}\frac{\partial[(1-c)hT_{xx}]}{\partial x}+\frac{1}{\rho}\frac{\partial[(1-c)hT_{xy}]}{\partial y}-\frac{\tau_{bx}}{\rho}-\frac{f_{vx}h}{\rho} \quad (2)$$

$$\frac{\partial[(1-c)vh]}{\partial t}+\frac{\partial[(1-c)uvh]}{\partial x}+\frac{\partial[(1-c)vvh]}{\partial y}$$
$$=-g(1-c)h\frac{\partial z_s}{\partial y}+\frac{1}{\rho}\frac{\partial[(1-c)hT_{yx}]}{\partial x}+\frac{1}{\rho}\frac{\partial[(1-c)hT_{yy}]}{\partial y}-\frac{\tau_{by}}{\rho}-\frac{f_{vy}h}{\rho} \quad (3)$$

where t is the time; x and y are Cartesian coordinates in a

horizontal plan; h is the flow depth; u and v are the depth-averaged flow velocities in the x- and y-directions, respectively; z_s is the water surface elevation; g is gravity; c is porosity; T_{xx}, T_{xy}, T_{yx}, and T_{yy} are the depth-averaged turbulent stresses; τ_{bx} and τ_{by} are the x- and y-components of the bed shear stress, respectively; ρ is the water density; and, f_{vx} and f_{vy} are the x- and y-components of the drag force exerted on the groins per unit volume, respectively. Equations (1) to (3) reduce to the free flow condition as the permeable pile groins disappear ($c \to 0$). The bed shear stresses are determined by

$$\tau_{bx} = \rho(1-c)c_f \; u \; |U| \tag{4}$$

$$\tau_{by} = \rho(1-c)c_f \; v \; |U| \tag{5}$$

where $|U|$ is the velocity magnitude calculated by $|U| = \sqrt{u^2 + v^2}$, and c_f is the friction coefficient determined by $c_f = gn^2 / h^{1/3}$, n is Manning's coefficient.

The eddy-viscosity concept, which is used to estimate the quantities of turbulent stresses, is expressed as

$$T_{xx} = 2\rho(\nu + \nu_t)\frac{\partial u}{\partial x} - \frac{2}{3}k \tag{6}$$

$$T_{xy} = T_{yx} = 2\rho(\nu + \nu_t)(\frac{\partial u}{\partial y} + \frac{\partial v}{\partial x}) \tag{7}$$

$$T_{yy} = 2\rho(\nu + \nu_t)\frac{\partial v}{\partial y} - \frac{2}{3}k \tag{8}$$

where ν is the kinematic viscosity of water, ν_t is the eddy viscosity due to turbulence, and k is the turbulence energy. Eddy viscosity ν_t is a function of k and its rate of dissipation is ε. ν_t is expressed as

$$\nu_t = c_\mu \frac{k^2}{\varepsilon} \tag{9}$$

where c_μ is an empirical constant. Subsequently, transport equations are required for k and ε to close the problem. Selecting an appropriate $k-\varepsilon$ turbulent model is a source of considerable ambiguity and inconsistency in published work. We assume turbulent diffusive effects are dominated by source terms within momentum equations. Thus, the $k-\varepsilon$ turbulent model is not modified and source terms required for fluid-groin interactions are only incorporated in momentum equations. The following transport equations for k and ε are solved:

$$\frac{\partial k}{\partial t} + u\frac{\partial k}{\partial x} + v\frac{\partial k}{\partial y} = \frac{\partial}{\partial x}\left[\frac{\nu_t}{\sigma_k}\frac{\partial k}{\partial x}\right] + \frac{\partial}{\partial y}\left[\frac{\nu_t}{\sigma_k}\frac{\partial k}{\partial y}\right] + P_h + P_{kv} - \varepsilon \tag{10}$$

$$\frac{\partial \varepsilon}{\partial t} + u\frac{\partial \varepsilon}{\partial x} + v\frac{\partial \varepsilon}{\partial y} = \frac{\partial}{\partial x}\left[\frac{\nu_t}{\sigma_\varepsilon}\frac{\partial \varepsilon}{\partial x}\right] + \frac{\partial}{\partial y}\left[\frac{\nu_t}{\sigma_\varepsilon}\frac{\partial \varepsilon}{\partial y}\right] + c_1\frac{\varepsilon}{k}P_h + P_{\varepsilon v} - c_2\frac{\varepsilon^2}{k} \tag{11}$$

where c_1, c_2, σ_k, and σ_ε are empirical coefficients. The following functions for P_h, P_{kv}, and $P_{\varepsilon v}$ are applied

$$P_h = \nu_t\left[2\left(\frac{\partial U}{\partial x}\right)^2 + 2\left(\frac{\partial V}{\partial y}\right)^2 + \left(\frac{\partial U}{\partial y} + \frac{\partial V}{\partial x}\right)\right] \tag{12}$$

$$P_{kv} = \frac{1}{c_f^{1/2}}\frac{u_*^3}{h} \tag{13}$$

$$P_{\varepsilon v} = 3.6\frac{c_2}{c_f^{3/4}}c_\mu^{1/2}\frac{u_*^4}{h^2} \tag{14}$$

with bed shear velocity determined by

$$u_* = c_f^{1/2}|U| \tag{15}$$

To avoid any calibration of simulations for different flow situations, standard values (Rodi, 1993) of k and ε transport equations are used and given by:

$c_\mu = 0.09$, $c_1 = 1.44$, $c_2 = 1.92$, $\sigma_k = 1.0$, and $\sigma_\varepsilon = 1.3$.

DRAG FORCE ON PERMEABLE PILE GROINS

The problem of permeable pile groins presented here is similar to the flow passing vertical objects with a cylindrical shape. Generally, the drag of cylindrical elements can be parameterized by drag coefficients, cylindrical characteristics and flow characteristics. In the present study, a sink term to account for the drag of the stands of permeable pile groins is introduced into the Navier–Stokes equations. The term modified from the classical formula for flow around a cylinder and the drag force of the groins can be calculated. The following equations are used to demonstrate drag forces exerted on permeable pile groins per unit volume as:

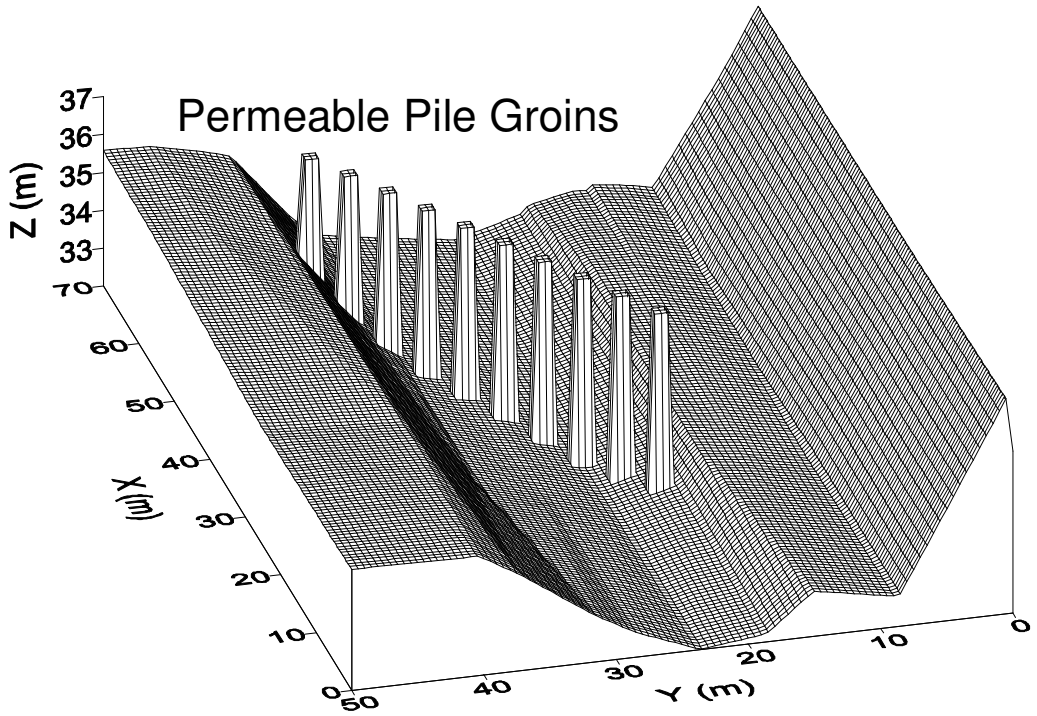

Figure 2. Computational mesh at study reach. View facing downstream.

$$f_{vx} = C_d \rho \alpha_v \frac{2c}{\pi D} |U| \; u \tag{16}$$

$$f_{vy} = C_d \rho \alpha_v \frac{2c}{\pi D} |U| \; v \tag{17}$$

where C_d is the drag coefficient, which is related to the flow and groin characteristics, α_v is a shape factor for the permeable piles, which accounts for the irregularity of pile groins (α_v =1 for a rigid pile groin), and D is the diameter of the groin.

During the computations, the mesh is generated first and then the porosity c is varied so that the property of the computational node equals that defined by the mesh geometry.

Numerical simulation

For the aforementioned set of governing equations, the boundary conditions for the inlet, outlet and wall are needed. The inlet boundary is considered as a Dirichlet boundary and flow discharge and water depth are prescribed at the entrance. The exit is selected far from the groin area and a Neumann boundary with zero gradients is introduced. Near a solid boundary ("wall") there is a viscous sublayer of flow where the velocity gradient is very large. The wall function approach, recommended by Rodi (1993), is applied to reduce the computational effort arising from resolving the viscous sublayer near the wall. The control-volume method of Patankar (1980) based on an orthogonal Cartesian coordinate system, is applied to discretize the governing equations. The numerical procedure SIMPLE introduced by Patankar (1980) is used to handle the pressure-velocity coupling in order to ensure conservation of mass. A non-uniform grid system with a large concentration of nodes in regions close to the groins is employed. The computational conditions in this study, including boundary conditions and permeable pile groin conditions, were set to match the conditions of the experiment. A computational mesh representing the study reach was constructed (Figure 2), and the experiment was numerically simulated.

RESULTS AND DISCUSSION

Figures 3 and 4 show measured and predicted depth-averaged velocities at cross sections A1 and A2 during the experiment with a discharge of 34.60 cm. Prediction of flow velocities is inferior, with the degree of agreement depending on the locations. In the cross section just upstream of the pile groins (A1), the prediction gives slightly higher values than the measured data. In the cross section just downstream of the pile groins (A2), the model agrees well with the measured data at the locations of Y = 0 – 25 m, while larger quantitative differences are found at the locations of Y = 25 – 35 m. This may be due to the locations of Y = 25 – 35 m at the cross section A2 being very close to the pile groins where the flow becomes complex and locally dominated by three-dimensional effects. This will make prediction by applying the depth-averaged numerical model difficult. However, it can still be seen that the trend predicated by the developed model is close to the measured data. The predicted velocity vector fields around the permeable pile groins under the

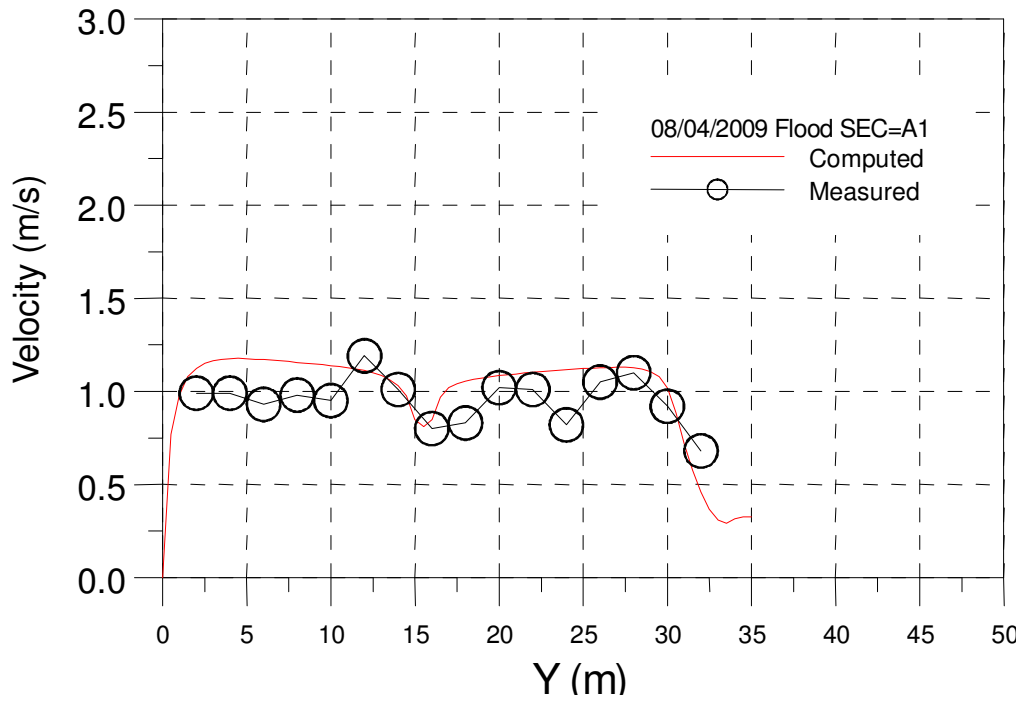

Figure 3. Comparison of measured and predicted velocities at cross section A1.

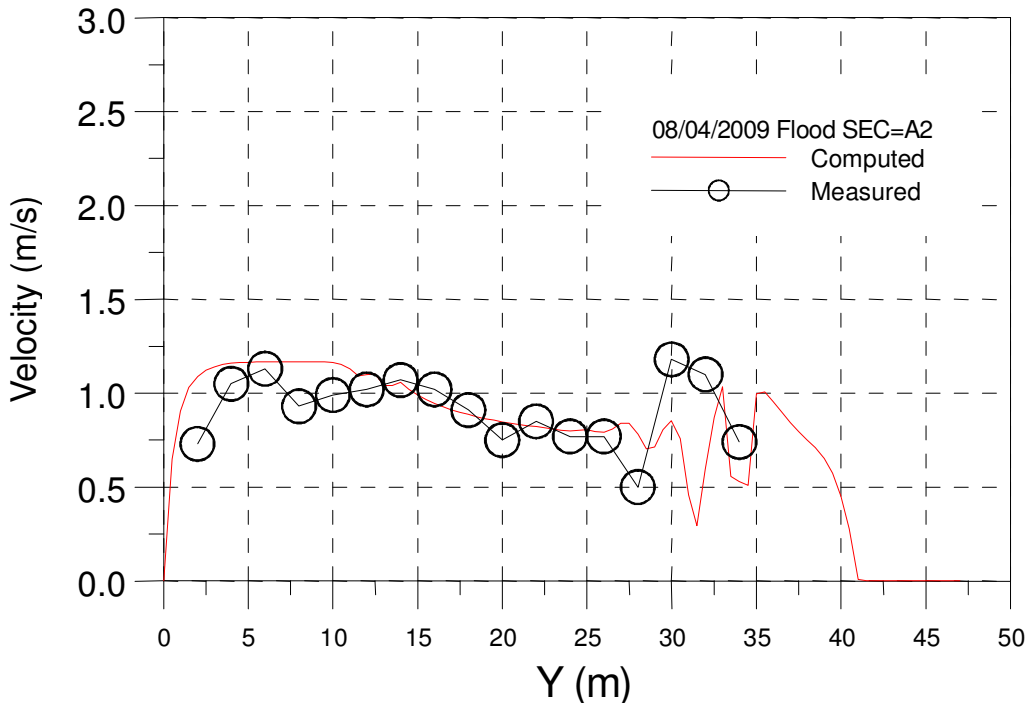

Figure 4. Comparison of measured and predicted velocities at cross section A2.

experimental condition are shown in Figure 5. The approaching flow is retarded by the permeable pile groins along the left bank and accelerated in the main channel near the right bank. Generally, a region with negative streamwise velocities behind solid groins is termed as a re-circulating region (Ahmed and Rajaratnam, 2000).

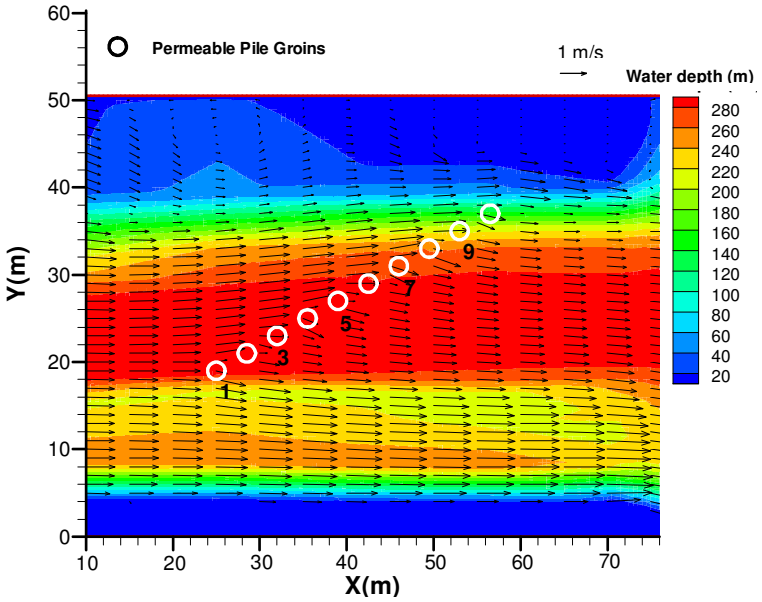

Figure 5. Predicted flow field at the study reach (Laonong River, Southern Taiwan; Discharge = 34.60 cm).

However, no re-circulating region exists behind the permeable pile groins. The predicted velocity vector fields is extremely useful for the explanation of how the flow passing the permeable pile groins, which is difficult to experimentally assess the hydrodynamic processes. The driving force for the recirculation is the momentum transfer in the horizontal plane. The jet flows passing through the gaps between the permeable pile groins prevent the formation of a re-circulating flow. With the permeable pile groins used here, the flow is driven by the momentum of the jet flows results in a parallel flow pattern when compared with that of solid groins.

Since in practice, groins are often flooded with different flow discharge, it is important to study the hydrodynamic effects of different flow conditions. The present numerical model is set to run for different discharges. The flow discharges are selected and equal to 10, 30, and 60 cm to represent low, medium and high flow conditions of the study reach, respectively. Figures 6a to c show variations of velocity vector fields at three flow conditions. These results give the qualitative and quantitative observations of flow patterns. When the flow approaches the upstream of the groins, the majority of the obstructed flow is diverted which causes a low velocity region just behind the groins. It can also be seen that just upstream of the groins, the flow direction diverts to the left bank with increasing the discharge. This can be an advantage for river bank protection because it reduces the flow velocity of the other bank. In all the cases investigated here, the momentum transfer by the water flowing through the permeable pile groins prevents the formation of a re-circulating flow. This momentum transfer also results in a drop of water depth when flow passes through the permeable pile groins. However, the drop of water depth decreases as the flow discharge increases. This is due to the jet flows passing through the gaps between the permeable pile groins becoming more pronounced as the flow discharge increases. The momentum transfer introduced by the jet flows enhances the flow motion behind the groins. Compared with the corresponding velocity of the approaching flows, the velocity reductions of flow passing through the groins are 40, 35 and 33% for discharges equal to 10, 30, and 60 cm, respectively. With the flow discharge used here, the high flow through the groins is rather uniform.

Conclusions

This study presents the results obtained from a numerical simulation of depth-averaged two-dimensional turbulent open channel flow passing through permeable pile groins. To determine the drag force exerted by the permeable pile groins, the model calculates the velocity within the groins by adding source terms into momentum equations. The generation of turbulence due to high flow conditions is also considered. The present numerical tool has been validated, incorporating *in-situ* experimental data and numerical results. The developed model shows a good qualitative and quantitative agreement with the experimental observations. Notably, the present model approach provides an efficient way to study the problem of flow passing through permeable pile groins. Additional results of the numerical simulation of the study reach with different flow discharges are presented mainly for the investigation of the hydrodynamic characteristics of

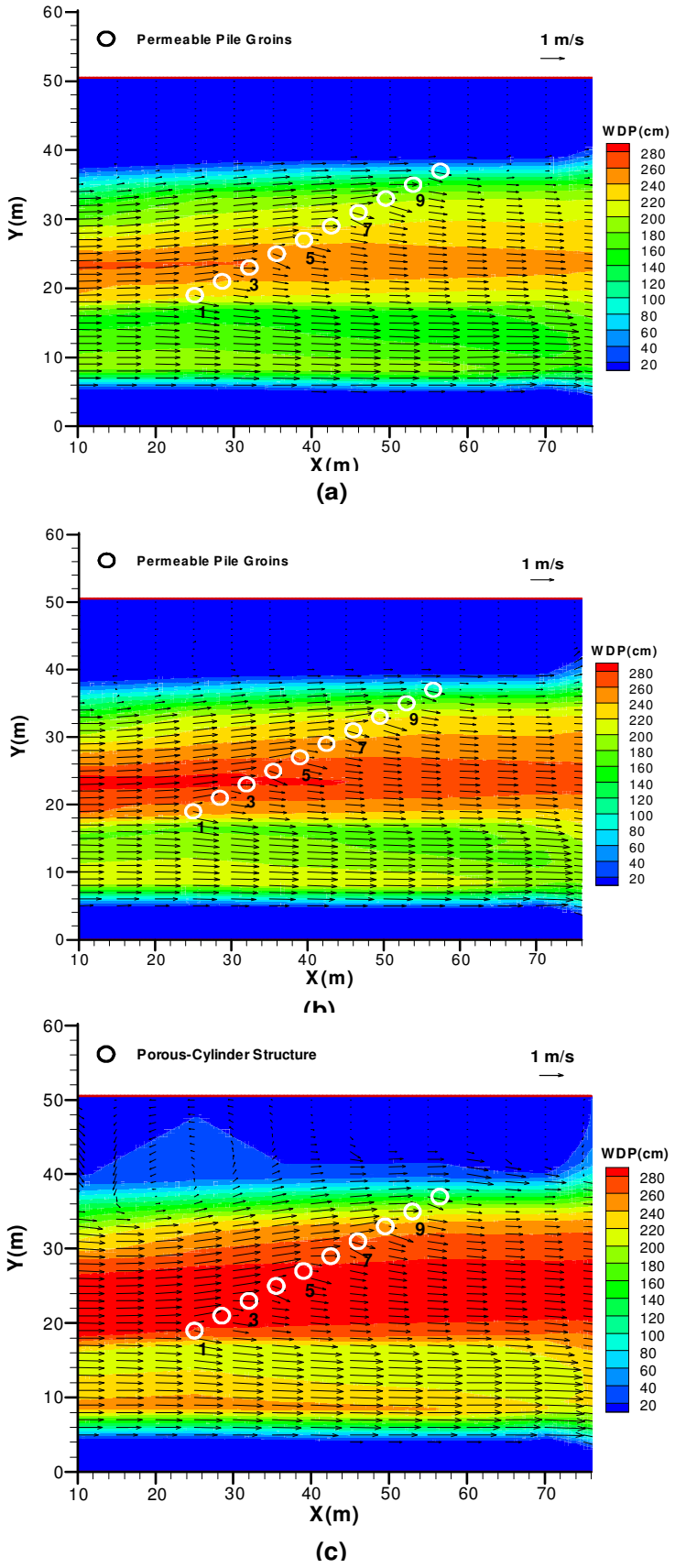

Figure 6. Predicted flow fields under different discharges at the study reach: (a) Discharge = 10.00 cm; (b) Discharge = 30.00 cm; (c) Discharge = 60.00 cm.

permeable pile groins. The numerical results show that the flow direction of an approaching flow is diverted while increasing the flow discharge. This can be an advantage for river bank protection because it reduces the flow velocity of the other bank. It was found that momentum transfer resulting from the jet flows passing through the gaps between the permeable pile groins became more pronounced as the flow discharge increased.

ACKNOWLEDGEMENT

This work was financially supported in part by the Water Resources Agency (WRA), Ministry of Economic Affairs (MOEA) of Taiwan.

REFERENCES

Abam TKS (1993). Control of channel bank erosion using permeable groins. Environ. Geol., 22(1): 21-25.

Abam TKS (1994). Factors affecting performance of permeable groins in channel bank erosion control. Environ. Geol., 26(1): 53-56.

Ahmed F, Rajaratnam N (2000). Observations on Flow Around Bridge Abutment. J. Eng. Mech. ASCE, 126(1): 51-59.

Arlinghaus R, Engelhardt C, Sukhodolov A, Wolter C (2002). Fish recruitment in a canal with intensive navigation: Implications for ecosystem management. J. Fish. Biol., 61(6): 1386-1402.

Armstrong JD, Kemp PS, Kennedy GJA, Ladle M, and Milner NJ (2003). Habitat requirements of Atlantic salmon and brown trout in rivers and streams. Fish. Res., 62(6): 143-170.

Barbhuiya AK, Dey S (2004). Turbulent flow measurement by the ADV in the vicinity of a rectangular cross-section cylinder placed at a channel sidewall. Flow Meas. Instrumt., 15(4): 221-237.

Bischoff A , Wolter C (2001). Groyne-heads as potential summer habitats for juvenile rheophilic fishes in the lower Oder, Germany. Limnologica, 31: 17-26.

Carling PA, Kohmann F, Golz E (1996). River hydraulics, sediment transport and training works: their ecological relevance to European rivers. Archiv. Hydrobiol. Suppl., 113(10): 129-146.

Huang YR (2001). Observations of scour and deposit of the in-line Porous Basket groups in the channel. Master thesis, Dept. of Hydraulic & Ocean Engineering, National Cheng Kung University, Taiwan (in Chinese).

Jia Y, Wang SSY (1996). A modeling approach to predict local scour around spur dike-like structures. Proc., 6th Federal Interagency Sedimentation Conf., Subcommittee on Sedimentation, Interagency Advisory Committee on Water Data, 2: 90-97.

Kruk A (2007). Role of habitat degradation in determining fish distribution and abundance along the lowland Warta River, Poland. J. Appl. Ichthyol., 23(1): 9-18.

Kwan TF, Melville BW (1994). Local scour and flow measurements at bridge abutments. J. Hydraul. Res., 32(5): 661-673.

Leu JM, Chan HC, Jia Y, He Z, Wang SSY (2008). Cutting management of riparian vegetation by using hydrodynamic model simulations. Adv. Water Res., 31(10): 1299-1308.

Patankar SV (1980). Numerical heat transfer and fluid flow. New York: Hemisphere.

Rajaratnam N, Nwachukwu BA (1983). Flow near groin-like structures. J. Hydraul. Eng.-ASCE, 109(3): 463-480.

Rodi W (1993). Turbulence models and their application in hydraulics, 3rd Ed. The Netherlands: IAHR Monograph, Balkema, Rotterdam.

Schwartz R, Kozerski H (2003). Entry and deposits of suspended particulate matter in groyne fields of the middle Elbe and its ecological relevance. Acta Hydrochim. Hydrobiol., 31(4-5): 391-399.

Shields Jr FD, Cooper CM, Knight SS (1995). Experiment in stream restoration. J. Hydraul. Eng.-ASCE, 21(6): 494-502.

Teraguchi H, Nakagawa H, Muto Y, Baba Y, Zhang H (2008). Effects of groins on the flow and bed deformation in non-submerged conditions. Annuals of Disas. Prev. Res. Inst., Kyoto Univ., 51(B): 625-632.

Uijttewaal WSJ (2005). The effects of groyne layout on the flow in groyne fields : laboratory experiments. J. Hydraul. Eng.-ASCE, 13(9): 782-791.

Xu CJ, Cai YQ, Xuan WL, Chen HJ, Song Y (2006). *In-situ* Test and Numerical Analysis of Bore Pressure on Sheet-Pile Groin. China Ocean Eng., 20(3): 431-442.

Yazdi J, Sarkardeh H, Azamathulla HMD, Ghani AAB (2010). 3D simulation of flow around a single spur dike with free-surface flow. Intl. J. River Basin Manage., 8(1): 55-62.